Coastal Dynamics 2017
Paper No. 151

RUN-UP OF VERY LONG WAVES GENERATED BY BOTTOM-TILTING WAVE MAKER

Yong Sung Park[1]

Abstract

Motivated by the need to generate more realistic model tsunamis, a new wave maker has been developed at the University of Dundee. The wave tank is formed with an adjustable slope and a bottom flap hinged at the beginning of the slope. The new tank can generate both leading-elevation waves (LEW) and leading-depression waves (LDW), which are an order-of-magnitude longer than solitary waves for the same wave height-to-water depth ratio. In the present study, we report the maximum run-up heights of both LEWs and LDWs along a plane beach. While LEWs exhibit simple relationship between the maximum run-up height and the wave generation parameters, no such relation is found for LDWs. It was found that the maximum run-up heights for both types of waves can be described as a power function of the steepness of the accelerating phase of the wave at the point of wave generation.

Key words: tsunami, long waves, wave maker, run-up, experiment

1. Introduction

As tsunami approaches shore and run up on beach, its amplitude rapidly increases, resulting in loss of lives and properties. For instance, the tsunami that struck Sanriku, Japan in 1896, recorded 38 m of maximum run-up height and caused 22,000 casualties. The recent 2011 East Japan tsunami had the maximum run-up height of about 40 m, which resulted in 16,000 casualties (Mori and Takahashi 2012). Understanding run-up process and predicting maximum run-up height have been a key research objective in tsunamis research. In particular, solitary wave has been used as the model tsunami for the last few decades and numerous studies on run-up of solitary waves are found in literature (e.g. Hall and Watts 1953, Synolakis 1987, Zelt 1991, Briggs et al. 1995, Jensen et al. 2003, Lo et al. 2013 and the references within).

On the other hand, it is now widely accepted that solitary waves are just too short to properly model tsunamis (Madsen et al., 2008), which requires development of novel long wave generation methods. In response to this call, there now are a number of publications available in literature. For example, Rossetto et al. (2011) used a pneumatic pump to release volume of water into wave basin in a controlled manner, and Goseberg et al. (2013) developed a close-circuit wave flume in which waves are driven by pipe pumps for virtually arbitrary surface profiles.

Recently, Lu et al. (2017a, b) presented another long wave generation method using so-called the bottom-tilting wave maker (figure 1). The wave tank is fitted with an adjustable slope and a bottom flap hinged at the beginning of the slope. By moving the bottom flap up and down, very long waves can be generated. By carefully investigating the analytical solution of the linearised equations, the numerical solution of nonlinear equations (both Nonlinear Shallow Water Equations and Boussinesq equations) and experimental measurements, Lu et al. (2017a, b) demonstrated that the new wave maker is capable of generating waves that are orders-of-magnitude longer than the solitary wave. Furthermore long waves with both positive and negative fronts can be easily obtained.

In the present paper, we are particularly interested in the classic problem of wave run-up along a plane

[1]School of Science and Engineering, University of Dundee, Dundee DD5 3LE, United Kingdom.
y.s.park@dundee.ac.uk

beach. Our unique contribution for this problem is that run-up of very long waves with a variety of surface profiles are investigated. The experimental results are compared to available analytical and numerical conditions. It will be shown that wave-front profile at the toe of the beach is a good predictor of the run-up height.

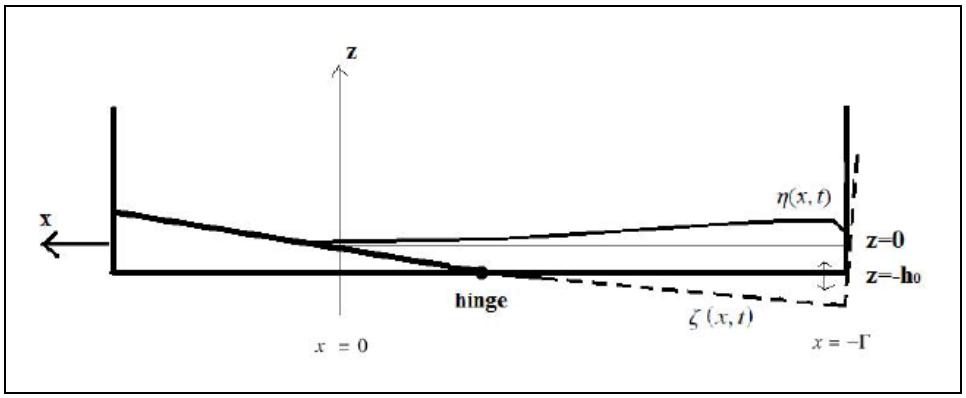

Figure 1. Schematic diagram of the bottom-tilting wave maker.

In the next section, experimental setup will be used, followed by experimental results in section 3. Analysis of the data, in particular, the simple relationship between the run-up height and the wave-front profile is discussed in section 4. Finally, concluding remarks are presented in section 5.

2. Experimental set-up

Experiments were carried out in the bottom-tilting wave tank (2 m long, 0.1 m wide and 0.2 m high). The bottom of the tank consists of two parts: 1-m-long fixed part and 1-m-long flapping part. The hinge of the flapping bottom is at the junction of the two bottom parts. The slope of the fixed bottom part can be adjusted. Figure 2 shows a photograph of the experimental set-up around the wave tank.

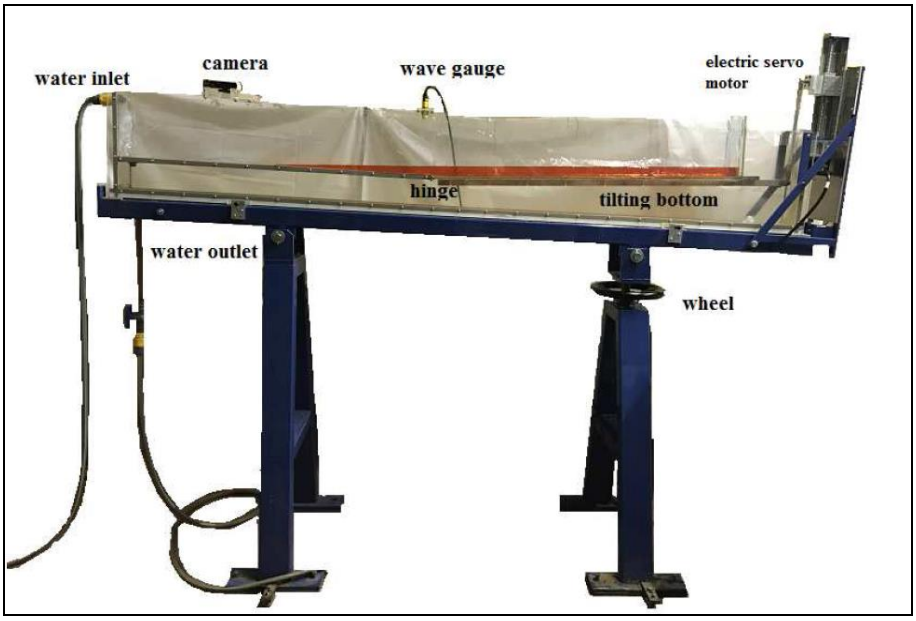

Figure 2. A Photograph of the wave tank used for the experiments.

The moving bottom was actuated by a computer-controlled electrical servo motor (ANIMATICS® SM23165DT). An acoustic wave gauge (BANNER® U-STAGE™ S18UUA) was used to measure the free surface elevation at the toe of the beach. The frequency of the wave gauge was set at 50 Hz with the accuracy of ±0.5 mm. The run-up process was recorded by a compact camera (CASIO® EXILIM ZR3500) mounted overhead of the beach and parallel to the beach. The camera can record movies at the rate of 30 frames per second and with the resolution of 640×480 pixels per frame. Grid lines with 2 cm spacing are marked just beneath the perspex beach so that the trajectory of the shoreline can be obtained from the recorded movies (figure 3).

Figure 3. Measurements of run-up using a grid and a compact camera

The maximum run-up can be decided by finding the furthest location wave front can reach, whose exact location is found by interpolation between two nearest grid lines. Also we note here that the run-up height is measured vertically from the initial shoreline.

2.1. *Notation and nondimensionalisation*

The two-dimensional Cartesian coordinate system is shown in figure 1, in which the origin is placed at the initial shoreline. The horizontal x axis is positive onshore, and the vertical z axis increases upward. The free surface is located at $z = \eta(x, t)$ and the initial horizontal length of the domain is defined as Γ, so that the offshore end of the tank is located at $x = -\Gamma$. The slope of the plane beach is denoted as γ, and the time axis t. The time-varying bathymetry is at $z = -h(x, t)$, where $h(x, t) = h_0 + \zeta(x, t)$, h_0 is the initial water depth in the offshore and ζ is the displacement of the moving bottom.

We also denote the length of the moving bottom as L; the wave amplitude, A; the wave period, T; and the maximum wave run-up height, R_m, respectively. Hereinafter, it is understood that variables are nondimensionalised using h_0 and $(gh_0)^{1/2}$ as the characteristic length scale and the characteristic time scale, respectively, where g is the gravitational acceleration. Also we define a nondimensional depth parameter, $\alpha = h_0 L^{-1}$, to indicate experimental results carried out at different initial water depths.

2.2. *Wave generation*

Two types of waves were used, namely leading-elevation and leading-depression waves. A leading-elevation wave (LEW) is generated by moving the bottom flap upward at a constant speed from the initial negative displacement $\zeta(L, 0) = -a$ to flat position $\zeta(L, b) = 0$ over the duration b. On the other hand the leading-depression wave (LDW) was generated by initiating the bottom motion from flat position $\zeta(L, 0) = 0$ downward at a constant speed to the maximum negative displacement $\zeta(L, b) = -a$ and moving it back at the same speed to the flat position $\zeta(L, 2b) = 0$.

Figure 4 shows examples of LEWs and LDWs, in which numerical results are calculated by solving

nonlinear shallow water equations as described in Lu et al (2017a). Good agreement between the experimental measurements and numerical simulations observed in the figure ensures both the quality of experimental data and the performance of the numerical scheme.

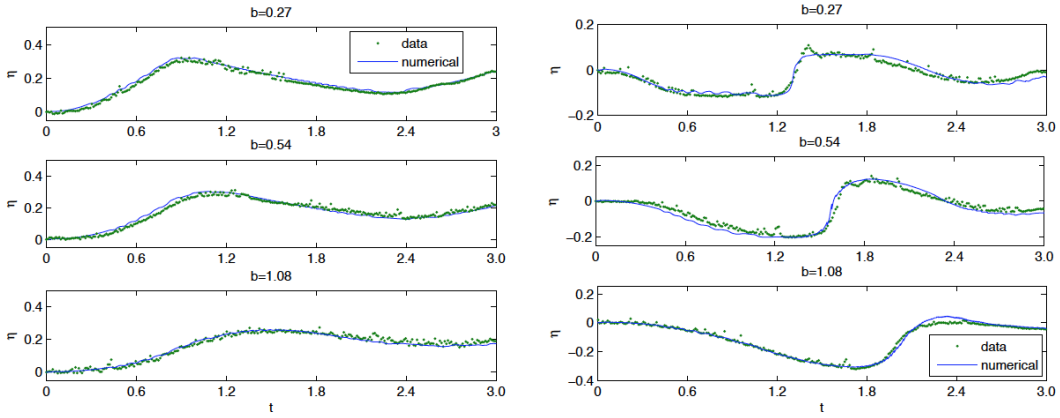

Figure 4. Typical waves used in the present research. Left: leading-elevation waves; right: leading-depression waves.

All the cases shown in figure 4 were generated with the beach slope γ = 1/20, the water depth α = 0.03 and the bottom motion amplitude a = 0.67. It is interesting to note that while the wave amplitudes of LEWs decrease with increasing b, no such simple relationship can be found for LDWs. This point will be further discussed in later parts.

2.3. *Experimental cases*

Three different beach slopes were used, namely γ = 1/15, 1/20 and 1/25. For each of the beach slope and each type of the waves (i.e. LEW and LDW), 52 experimental cases were tested, by varying α, a and b (see table 1), a total of 312 cases.

Table 1. Experimental cases for each of three beach slopes.

α	a	b
0.020	0.25, 0.50, 0.75, 1.00	0.22, 0.44, 0.66, 0.89
0.025	0.20, 0.40, 0.60, 0.80	0.25, 0.50, 0.74, 0.99
0.030	0.17, 0.33, 0.50, 0.67, 0.83	0.27, 0.54, 0.81, 1.09

We note here that each experimental case was repeated at least three times to ensure the repeatability.

3. Experimental results

3.1. *Run-up heights*

The maximum run-up height R_m can be obtained by capturing the furthest offshore location from the time history of the shoreline. The experimental results of the maximum run-up height of the long waves on the plane beach with γ = 1/20 are plotted against the bottom motion amplitude a and the duration b in figure 5 for both LEW and LDW, respectively. We remark here that waves have greater R_m on gentler beaches, but otherwise similar trends as in figure 5 are observed. Therefore the experimental data for the other two beach slopes are not shown for the sake of brevity.

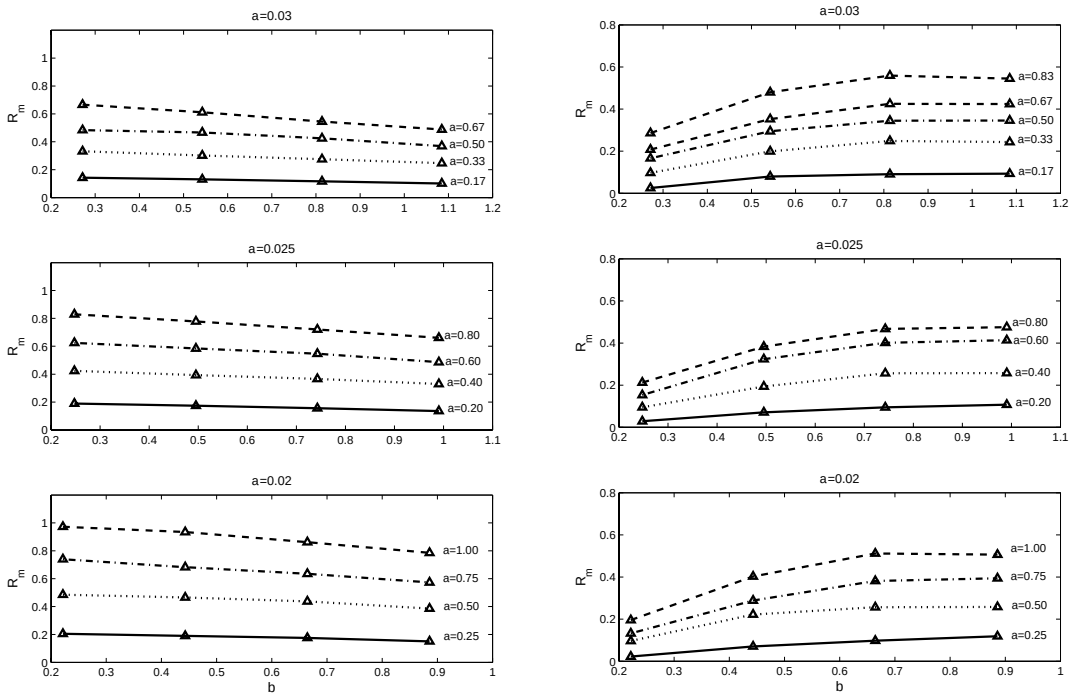

Figure 5. The maximum run-up height plotted against varying a and b with $\gamma = 1/20$. Left: leading-elevation waves; right: leading-depression waves for LEWs.

First, let us focus on the relation between the motion parameters and the maximum run-up height for LEWs. It is observed that R_m increases with increasing motion amplitude a, but opposite trends are found for the motion duration b. Obviously, greater motion displacement drives more water to uprush the beach, which results in a greater run-up height. Indeed Lu et al. (2017b) showed that the wave amplitude is proportional to the volume flux of the displaced water by the moving bottom. The shorter the motion duration, the greater the speed of the moving bottom and the displaced water, which imparts greater energy to the waves and results in the higher wave run-up height. We also remark that regardless of duration, the volume of displaced water is solely determined by the initial bottom displacement a, which is not the case for LDWs as will be discussed below.

As explained in section 2.2, the LDWs were generated by lowering the bottom flap from initially flat position to a certain distance and then by raising it back to the flat position at a constant speed. Unlike the LEWs, the volume of the displaced water is now dependent on both bottom motion amplitude a, and the duration b. It is because the water initially on the beach will be drained into the lowered bottom and the right panels in figure 5 show that the maximum run-up height R_m increases with increasing b to a certain point. It may be observed in figure 4 that the wave height and the volume of the displaced water show a similar tendency. However, the increasing trend turns to a slight drop at the greatest b and a for all the three values of α. The slower increasing trend observed in the figure may be explained by the elongation of the wave profile by slow bottom motion which reduces the wave front steepness and the wave height. However, elongation is not the only cause since the drop of the increasing trend of R_m with b becomes obvious for bigger motion amplitude.

Let us further consider the drop of the increasing trend of the maximum run-up height R_m with respect to b. In figure 6, R_m of the high-amplitude waves generated by the down-and-upward motions with the biggest a for every α is plotted with respect to b and compared among the three beach slopes.

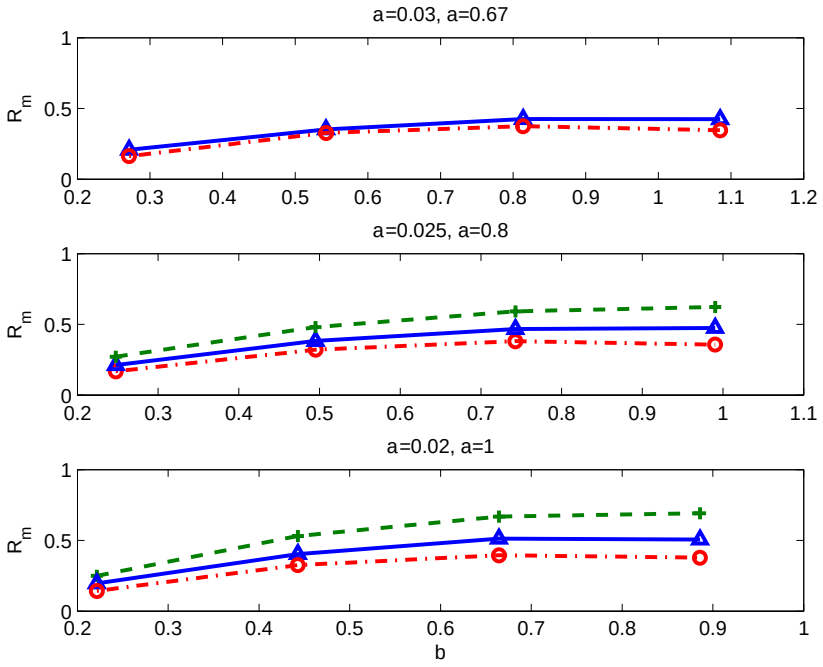

Figure 6. Experimental data of the maximum run-up height of the LDWs plotted against b with a = 0.67, a = 0.8 and a = 1.0, respectively: green crosses, γ = 1/25; blue triangles, γ = 1/20; red circles, γ = 1/15.

First, we note that there is lack of information of waves by the bottom motions with a = 0.67 for α = 0.03 and slope of 1/25 due to the limited length of the wave tank. For large b, it was observed during the experiments that the shoreline recedes from the beach to the offshore direction well before the bottom motion has completed. It is thought that too slow a bottom motion and a large motion displacement create more space for the water on beach to fill in. This in turn lowers the shoreline location before the arrival of the wave and reduces the maximum run-up height measured from the initial shoreline. That explains that the drop is much more obvious with greater a in figures 5 and 6. The drop becomes more obvious for steeper slopes because there is a greater height difference of the shoreline on steeper slope when same amount of water is lowered to fill the moving area. Additionally, figure 6 also demonstrates that greater run-up height is induced by gentler slope for LDWs.

3.2. *Wave profile of the leading wave*

Next we turn our attention to the wave profile. In particular, we establish how the bottom motion parameters a and b determine wave profile and again its effects on run-up heights.

Wave profile especially for the accelerating phase of the wave is of great interest in this subsection with respect to the wave front steepness and the wave height for both LEWs and LDWs. As Chan and Liu (2012) have noted in their study, the back-profiles of the elevation part of the waves are not important when predicting the maximum run-up height. Therefore we only take the wave profile of the accelerating phase into consideration. Tadepalli and Synolakis (1994) also mentioned in their study that the N-waves have the same run-up height to the solitary waves with the same accelerating profile and wave height regardless of the back-profiles. Indeed, according to the analytical solution proposed by Madsen et al. (2008), it can be clearly found that the gradient of the wave profile with respect to time plays a crucial role in estimating the time histories of the run-up height.

Here, the accelerating phase is determined as the part of the profile from the beginning to the wave crest for the LEWs and from the wave trough to the crest for the LDWs, respectively. Then, the steepness of the

accelerating phase is defined as $\kappa = (\eta_{peak} - \eta_{nadir}) / (t_{peak} - t_{nadir})$, indicating that greater κ leads to a steeper wave front.

As the waves generated by the bottom-tilting wave maker is very long compared to the length of the wave tank, the effects of the reflected waves are felt in very early stages of experiments. It becomes even more evident with sloping beach in place in the tank. Therefore we used data from numerical simulation in semi-infinite domain with flat bottom to calculate κ at the moment of wave generation and at the hinge. The good agreement between the experimental data and the numerical simulation shown in figure 4 and in Lu et al. (2017a, b) may justify the practice. The resulting wave front steepness κ of all the incident waves are presented in figure 7 as a function of a and b.

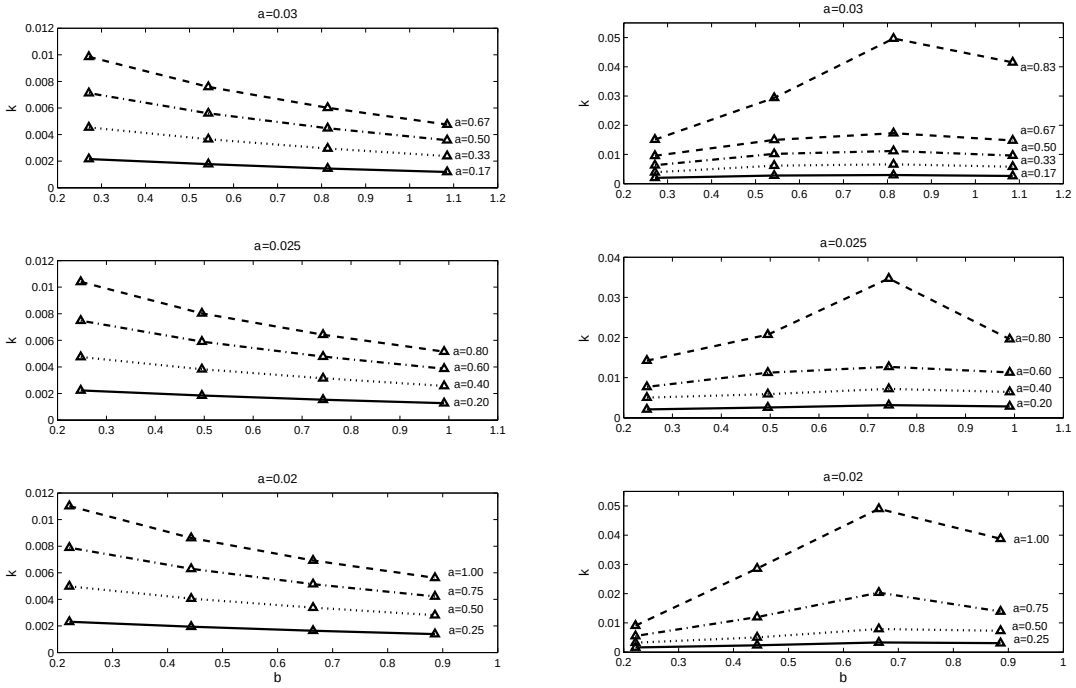

Figure 7. Plot of the wave front steepness against varying a and b. Left: leading-elevation waves; right: leading-depression waves.

It is very interesting to observe in figure 7 that κ behaves almost the same to how R_m trends with the varying bottom motion parameters a and b. Greater motion amplitude leads to steeper wave front, for both LEWs and LDWs. Wave front steepness decreases with the increasing motion duration time for the LEWs, but there is no monotonous dependence that relates κ and b for LDWs. Similar to the trends observed on the right panel in figure 5, the increasing trend slows down and even drops at greater a and b for the LDWs. Thus, it suggests that the wave front steepness at the point of wave generation is an important factor to predict the wave run-up height, which will be validated below.

4. Analysis and discussion

In this section, we aim to further investigate the role of the wave profiles of the accelerating phases of the waves in predicting the maximum run-up height. In figure 8, the maximum run-up heights are plotted against the wave front steepness for both LEWs and LDWs.

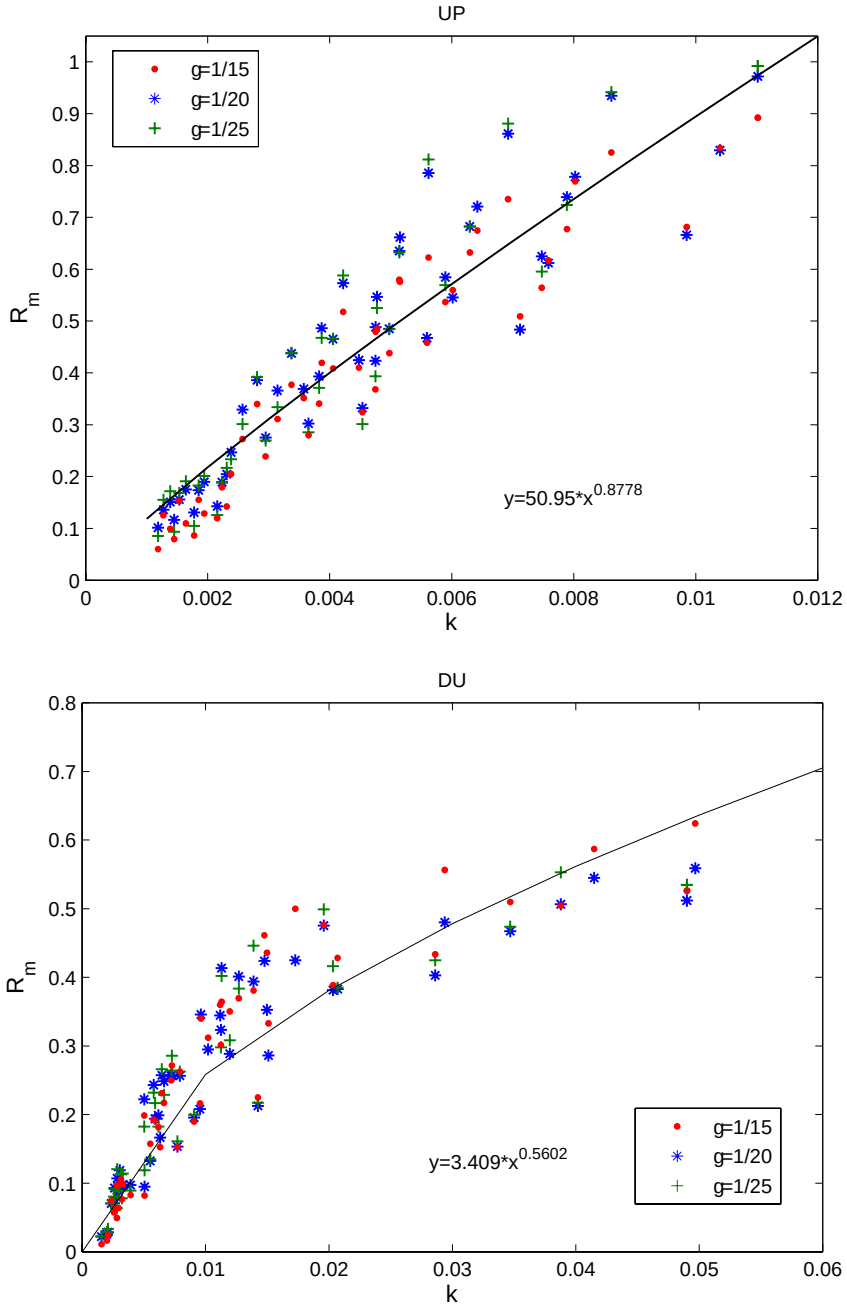

Figure 8. Experimental results of the maximum run-up height plotted as a function of the front steepness. Symbols, experimental data; solid line, fitted power function.

It is observed that R_m grows with the increasing κ. Although the results appear scattered for both types of waves, a power function fits the data very well. For LDWs, the gradient of the fitted curve slows down at around κ = 0.010. It may be caused by that the effects of the wave breaking become more significant, but more research are to be done. Also, the waves generated by upward motions have greater R_m than the waves by down-and-upward motions at the same κ. It is not only because of their different wave forms but also the different wave heights at the same steepness. Then, different wave heights of the waves at the same κ result in the scattering in the monotonous relation in figure 8.

5. Concluding remarks

Motivated by the question arising in recent research on the solitary wave paradigm for modelling tsunamis, we have designed a bottom-tilting wave maker aiming to generate very long waves (Lu et al. 2017a, b). In the present study, we have explored the evolution and run-up of the long waves generated in the new wave tank. The topography of the problem consists of a generation region with a moving bottom directly connected to a plane sloping beach whose slope is adjustable.

Experiments were conducted to measure the water surface elevation time histories, the shoreline moving trajectories and the maximum run-up heights in the laboratory. A compact camera installed above the beach of the tank has been used to observe the maximum run-up height of various waves. Meanwhile, a wave gauge has been used to measure the free surface elevation at the toe of the slope.

Theoretically, the run-up process and the maximum run-up height can be estimated by the numerical modelling based on nonlinear shallow water equations. The governing equations were solved by a high-order shock-capturing finite volume scheme (Lu et al. 2017a). In addition, the movement of the shoreline was approximated by the computational domain mapping technique. Since the numerical modelling has been verified by the experimental measurements, further observation of the wave front profile determined by numerical results are believed to be reliable.

We have further explored the effects of the bottom motion on the run-up of the generated long waves in terms of the increase in displaced water volume and the elongation of the wave profile for the cases with a slow motion of the moving bottom. Waves generated in the new wave maker have smaller maximum run-up height on a steeper beach. It has been verified that the steepness of leading wave front at the point of wave generation is a good predictor of the maximum run-up height for a single wave. The maximum run-up height can also be described by power functions of the wave front steepness. In general, high-amplitude wave with steeper wave front causes greater run-up height.

Acknowledgements

The author acknowledges financial support from the Royal Society of Edinburgh through the Royal Society of Edinburgh/Scottish Government Personal Research Fellowship Co-Funded by the Marie-Curie Actions.

References

Briggs, M. J., Synolakis, C. E., Harkins, G. S., and Green, D. R., 1995. Laboratory experiments of tsunami run-up on a circular island. In *Tsunamis, 1992–1994*: 569–593. Springer.

Chan, I.-C., and Liu, P. L.-F., 2012. On the runup of long waves on a plane beach. *Journal of Geophysical Research*, 117: C08006.

Hall, J. V. and Watts, G. M., 1953. *Laboratory investigation of the vertical rise of solitary waves on impermeable slopes.* Technical report, U.S. Beach Erosion Board.

Jensen, A., Pedersen, G. K., and Wood, D. J., 2003. An experimental study of wave run-up at a steep beach. *Journal of Fluid Mechanics*, 486(1): 161–188.

Lu, H., Park, Y. S. and Cho, Y.-S., 2017a. Modelling of long waves generated by bottom-tilting wave maker, *Coastal Engineering*, 122: 1-9.

Lu, H., Park, Y. S. and Cho, Y.-S., 2017b. Parametric investigation of long waves generated by bottom-tilting wave maker, *Coastal Engineering Journal*, (in revision).

Lo, H.-Y., Park, Y. S., and Liu, P. L.-F., 2013. On the run-up and back-wash processes of single and double solitary waves–an experimental study. *Coastal Engineering*, 80: 1–14.

Madsen, P. A., Furman D. R., and Schäffer, H. A., 2008. On the solitary wave paradigm for tsunamis. *Journal of Geophysical Research*, 113: C12012.

Mori, N. and Takahashi, T., 2012. Nationwide post event survey and analysis of the 2011 Tohoku earthquake tsunami. *Coastal Engineering Journal*, 54(01): 1250001.

Rossetto, T., Allsop, W., Charet, I., and Robinson, D. I., 2011. Physical modelling of tsunami using a new pneumatic wave generator. *Coastal Engineering*, 58: 517-527.

Synolakis, C. E., 1987. The runup of solitary waves. *Journal of Fluid Mechanics*, 185: 523–545.

Tadepalli, S. and Synolakis, C. E., 1994. The run-up of N-waves on sloping beaches. *Proceedings of the Royal Society of London A: Mathematical, Physical and Engineering Sciences*, 445: 99-112.

Zelt, J., 1991. The run-up of nonbreaking and breaking solitary waves. *Coastal Engineering*, 15(3): 205–246.